



# High contrast crystalline, dynamic, and excitation dependent room temperature phosphorescence by tuning acceptor structures

Weirao Ji<sup>a,1</sup>, Yupeng Zhao<sup>b,1</sup>, Yang Zhu<sup>a</sup>, Lei Ma<sup>b,\*</sup>, Yongtao Wang<sup>a,\*\*</sup>

<sup>a</sup> Guangxi Key Laboratory of Electrochemical and Magneto-chemical Function Material, College of Chemistry and Bioengineering, Guilin University of Technology, Guilin, 541004, China

<sup>b</sup> Tianjin International Center for Nanoparticles and Nanosystem, Tianjin University, Tianjin, 300072, China

## ARTICLE INFO

### Keywords:

Room temperature phosphorescence  
Dynamic phosphorescence  
Host-guest doping  
Long-lived phosphorescence  
Organic phosphorescence

## ABSTRACT

Donor-acceptor (D-A) type luminogens play an important role in constructing efficient organic room temperature phosphorescent (RTP) materials, whose RTP properties heavily depend on various D or A units. To screen for an excellent acceptor (A) unit and explore the inherent RTP mechanism, three organic phosphorescence luminogens (MBBe, MBCN and MBXAn) were prepared by choosing morpholine and Ph-CHO/CN/CONH<sub>2</sub> units as D and A respectively. Three luminogens and their doped films showed different crystalline, dynamic, and excitation dependent RTP. Among of them, crystal MBXAn emitted bright green afterglow, with RTP lifetime of 404.84 ms and RTP quantum yield ( $\Phi_p$ ) of 0.377, indicating excellent RTP performance. Crystal analysis and theoretical calculations confirmed that -CONH<sub>2</sub> unit could not only enhance intermolecular interactions, but also change molecular conformations of excited states, improve intersystem crossing (ISC) and RTP radiation rates. The work provided an excellent platform for building advanced encryption patterns by high contrast crystalline, dynamic, and excitation dependent RTP, and contributed to promoting a deeper understanding of RTP molecular design and intrinsic mechanisms.

## 1. Introduction

In recent years, room temperature phosphorescence (RTP) has attracted widespread attention due to unique excited state properties and long-lived delayed emission [1,2]. Compared with inorganic materials containing precious metals, pure organic RTP materials have potential application values in the fields of organic light-emitting diodes, oxygen sensing, biological imaging, and advanced data security because of their relatively lower cost and low toxicity, easy preparation, and high biocompatibility [3–12]. Promoting spin orbit coupling (SOC) between excited singlet and triplet states and suppressing non-radiative decay of triplet excitons are two important strategies to enhance RTP performance of organic materials, which mainly involves introducing heteroatoms, aromatic carbonyls, crystal engineering, copolymers, and host-guest doping systems [13–20]. Donor-acceptor D-A luminogens usually present small energy gap ( $\Delta E_{ST}$ ) between the lowest singlet ( $S_1$ ) and lowest triplet excited ( $T_1$ ) states, which is beneficial for boosting the intersystem crossing rate (ISC) and generating more triplet excitons,

thereby reducing the negative effects of non-radiative motion and triplet oxygen [21–28]. Even so, structure-RTP property relationships of the luminogens are still uncertain, while choosing different A units is very beneficial for making clear structure-RTP property relationship and obtaining efficient organic RTP luminogens.

With the further development of pure organic RTP materials, dynamic and color-tunable afterglow replacing long afterglow and high brightness have been new research hotspots, which can overcome the shortcomings of single color RTP in the past and promote the rapid development of high-level information encryption and anti-counterfeiting [29–32]. The reported literature indicates that non-traditional luminogens such as cellulose and sodium alginate easily showed excitation and time dependent colorful RTP due to the formation of diverse RTP emissive species, but there was still a lack of effective strategies to endow traditional conjugated aromatic compounds with the aforementioned colorful RTP [33–35]. Some luminogens with dual-band persistent thermally activated delayed fluorescence (TADF) and RTP achieved time dependent afterglow because of different TADF

\* Corresponding author.

\*\* Corresponding author.

E-mail addresses: [lei.ma@tju.edu.cn](mailto:lei.ma@tju.edu.cn) (L. Ma), [wyt\\_shzu@163.com](mailto:wyt_shzu@163.com) (Y. Wang).

<sup>1</sup> Contributed equally.



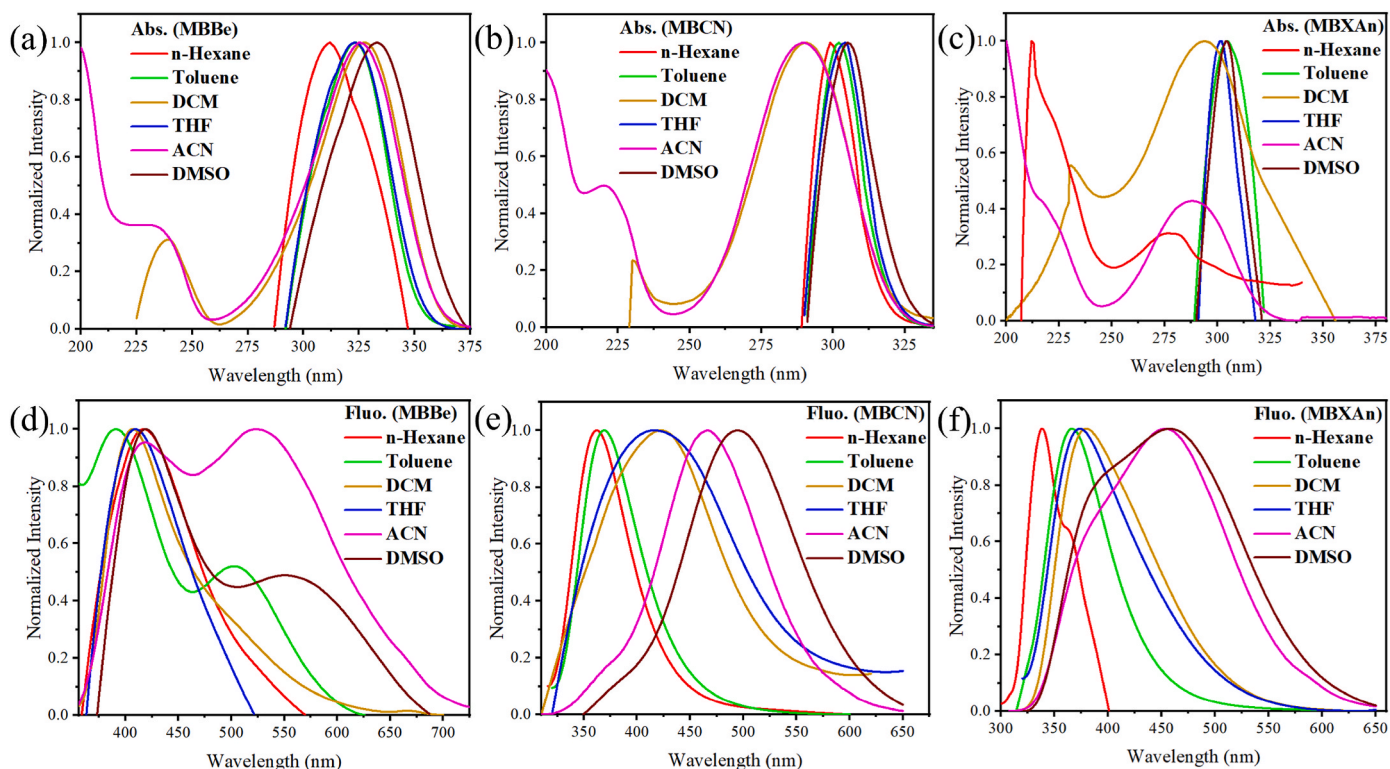


**Fig. 1.** UV-vis absorption spectra of (a) MBBE, (b) MBCN, (c) MBXAn and fluorescence emission spectra of (d) MBBE, (e) MBCN, (f) MBXAn in various solvents ( $10^{-5}$  M).

**Table 1**

Absorption and emission maxima, and the relative fluorescence quantum yields of MBBE, MBCN and MBXAn in different solutions.

		n-Hexane	Toluene	DCM	THF	ACN	DMSO
MBBe	Abs. (nm)	312	323	238, 327	322	232, 326	332
	$\lambda_F$ (nm)	417	390, 502	407	408	418, 523	418, 551
	$\Phi$ (%)	2.46	1.89	2.39	2.51	2.64	2.37
MBCN	Abs. (nm)	299	302	231, 291	304	220, 290	305
	$\lambda_F$ (nm)	362	368	421	416	466	495
	$\Phi$ (%)	1.95	2.43	4.87	4.38	5.01	5.24
MBXAn	Abs. (nm)	212, 278	304	231, 294	301	218, 288	304
	$\lambda_F$ (nm)	338, 365	366	380	374	390, 453	387, 457
	$\Phi$ (%)	3.06	7.36	7.57	7.44	9.23	9.54

**Table 2**

Emission maxima and quantum yields of three luminogens in doping films and solid states.

	$\lambda_{em}$		$\Phi$			
	Fluo. (nm)	Phos. (nm) ( $\lambda_{ex}$ :254 nm)	Phos. (nm) ( $\lambda_{ex}$ :365 nm)	Fluo. (%)	Phos. (%) ( $\lambda_{ex}$ :254 nm)	Phos. (%) ( $\lambda_{ex}$ :365 nm)
1 % MBBE@PVA	411	509	498	1.85	3.95	4.32
1 % MBCN@PVA	366	454	494	1.24	3.21	3.39
1 % MBXAn@PVA Pristine	372	454	470	2.32	5.81	6.39
1 % MBXAn@PVA After a week	372		496	2.32		8.95
MBXAn Powder	418		510	3.52		23.89
MBXAn Crystal	369, 412		496, 525	6.77		37.65

the observed dynamic afterglow, while RTP emission maxima of 1 % MBCN@PVA (454–494 nm) and 1 % MBXAn@PVA (454–496 nm) films continued to redshift as the excitation wavelength increased (Fig. 3a–c), indicating the presence of multiple RTP emission centers. Based on the (CIE: Commission International de l'Eclairage) CIE coordinates, RTP of 1 % MBBE@PVA film was located in the green light region, but RTP of 1 % MBCN@PVA and 1 % MBXAn@PVA films covered blue and green light regions (Fig. 3d–f). To understand dynamic afterglow of 1 % MBBE@PVA film, we measured its delayed RTP spectra at different delay times ( $\tau_d$ ). When  $\tau_d$  was 1 ms, 1 % MBBE@PVA film showed a strong emission peak at 520 nm and two weak emission peaks at 470 nm and 425 nm (Fig. S24a). The strong emission peak blue shifted to 512 nm, while the weak emission peaks at 470 nm and 425 nm disappeared and became a shoulder peak respectively when  $\tau_d$  was 5 ms and 10 ms. As  $\tau_d$  further increased to 30 ms, only the single strong emission peak with blue shifts of 3 nm remained. The delayed RTP spectra indicated that 1 % MBBE@PVA film also had multiple emission centers. Besides, the excitation spectra of 1 % MBBE@PVA film further confirmed the existence of multiple emission centers (Fig. S24b), displaying evident blue shifts and distinctions in excitation maxima and spectra. Obviously, the multiple emission centers should take responsible for dynamic afterglow of 1 % MBBE@PVA film. After being left at room temperature

**Table 3**  
The main photophysical parameters of MBXAn Powder and Crystal.

	$\tau$		k			
	Fluo. (ns)	Phos. (ms) ( $\lambda_{\text{exc}}$ :365 nm)	$k_{\text{Fl}}$ ( $\text{s}^{-1}$ )	$k_{\text{ISC}}$ ( $\text{s}^{-1}$ )	$k_{\text{Ph}}$ ( $\text{s}^{-1}$ ) ( $\lambda_{\text{exc}}$ :365 nm)	$k_{\text{Phnr}}$ ( $\text{s}^{-1}$ ) ( $\lambda_{\text{exc}}$ :365 nm)
MBXAn Powder	2.65	164.77	$1.33 \times 10^7$	$3.64 \times 10^8$	1.50	4.57
MBXAn Crystal	1.32	404.84	$5.13 \times 10^7$	$7.06 \times 10^8$	1.00	1.47

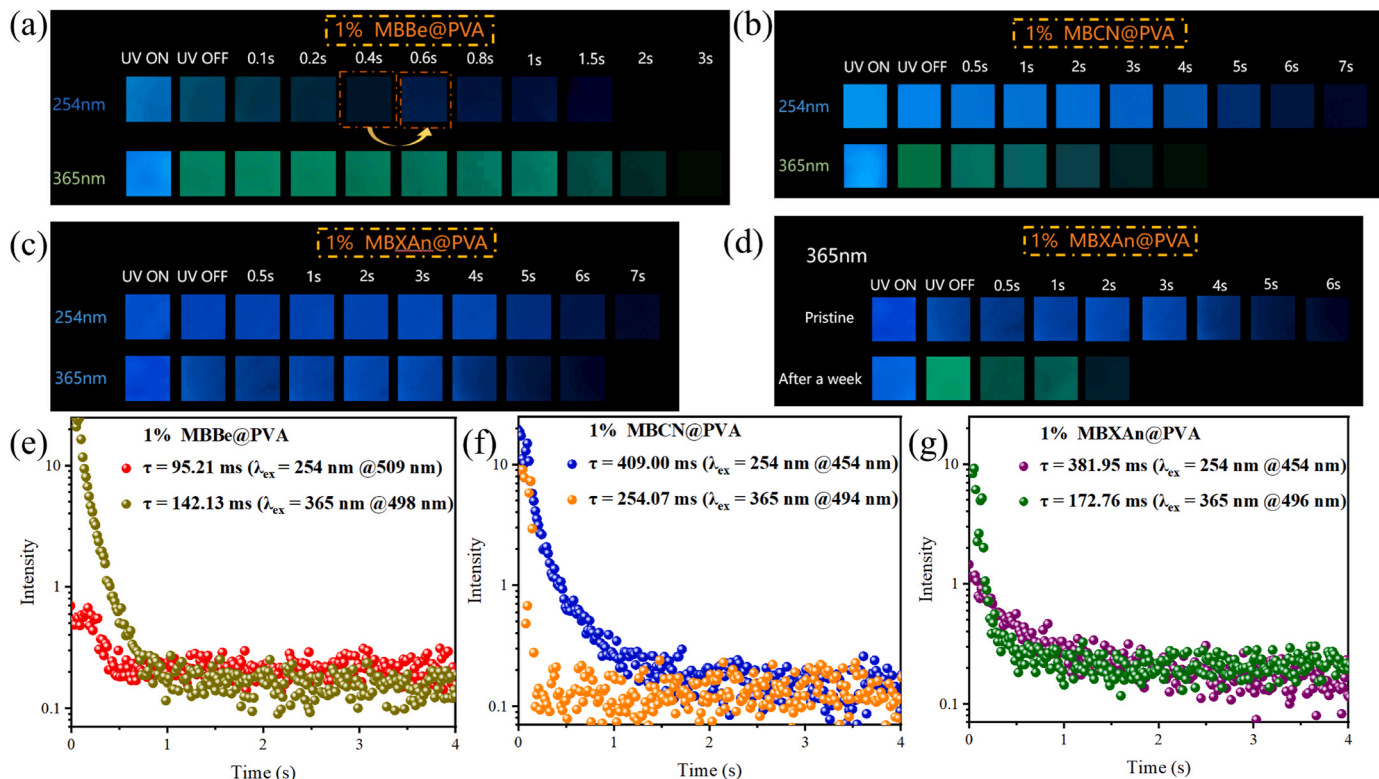


**Fig. 2.** (a)–(c) Photographs of 1 % MBBE@PVA, 1 % MBCN@PVA and 1 % MBXAN@PVA films by turning on/off 254 nm and 365 nm UV light lamps. (d) Photographs of 1 % MBXAN@PVA film by turning on/off 365 nm UV light lamps. (e)–(g) The time-resolved RTP decay curves of 1 % MBBE@PVA, 1 % MBCN@PVA and 1 % MBXAN@PVA films at 254 nm and 365 nm excitation.

for one week, 1 % MBXAN@PVA film showed green afterglow rather than blue afterglow by the switching on-off of 365 nm UV lamp, along with shortened afterglow lifetime (2 s) (Fig. 2d). It is widely known that luminogens can migrate and gather in PVA film, resulting in the coexistence of monomers and different aggregates. Therefore, the green afterglow of 1 % MBXAN@PVA film should be due to the presence of aggregated MBXAN, while the blue afterglow come from unimolecular MBXAN. Furthermore, the excitation spectra of the 1 % MBBE@PVA, 1 % MBCN@PVA, and 1 % MBXAN@PVA films were measured under different RTP maxima (Fig. S30), which showed excitation maxima of 324 nm and 327 nm for the 1 % MBBE@PVA film, 307 nm and 337 nm for the 1 % MBCN@PVA film, as well as 335 nm and 348 nm for the 1 % MBXAN@PVA film. This phenomenon further confirmed that the above dynamic and excitation dependent afterglow derived from the multiple emission centers constructed by unimolecular and aggregated luminogens. In addition, 1 % MBXAN@PVA film gave the highest  $\Phi_{\text{p}}$  (0.058), followed by 1 % MBBE@PVA (0.040) and 1 % MBCN@PVA (0.032) films under 254 nm excitation (Table 2). Under 365 nm excitation, the three doping films exhibited higher  $\Phi_{\text{p}}$ , but maintained the same increasing order from 1 % MBCN@PVA film (0.034) to 1 % MBBE@PVA (0.043) and 1 % MBXAN@PVA (0.064) films. Of note,  $\Phi_{\text{p}}$  of 1 % MBXAN@PVA film further increased to 0.090. Considering  $\Phi_{\text{p}}$  of power (0.239) and crystal MBXAN (0.377) again, the luminogens showed  $\Phi_{\text{p}}$  enhanced by aggregation and crystallization.

### 3. Crystal structures and theoretical calculations

To explore the underlying phosphorescence mechanism, crystal structures of MBCN (CCDC 2444411) and MBXAN (CCDC 2444412) were determined based on single-crystal X-ray diffraction and divided into planes O ( $\text{O}_1$ ,  $\text{C}_1$  and  $\text{C}_2$ ), A ( $\text{C}_1$ ,  $\text{C}_2$ ,  $\text{C}_3$  and  $\text{C}_4$ ), N ( $\text{N}$ ,  $\text{C}_3$  and  $\text{C}_4$ ), and B ( $\text{C}_5$ ,  $\text{C}_6$ ,  $\text{C}_7$ ,  $\text{C}_8$ ,  $\text{C}_9$  and  $\text{C}_{10}$ ) (Fig. 4). Dihedral angles of plane O–A and N–B were  $53.58^\circ$  and  $27.42^\circ$  successively in crystal MBCN, while crystal MBXAN showed more twisted molecular conjugation, corresponding dihedral angles are  $56.74^\circ$  and  $38.44^\circ$ . Furthermore, MBCN and MBXAN adopted side-to-plane arrangement modes (Fig. S25), without intermolecular  $\pi$ - $\pi$  stacking. As documented [41,43], the oxygen atom on the morpholine unit participates in stabilizing the molecular conformation through intermolecular interactions. More importantly, MBXAN relative to MBCN formed stronger and more intermolecular interactions by replacing CN with  $\text{CONH}_2$  (Fig. S26), which should be responsible for bright RTP of crystals MBXAN.

To reveal the inherent luminescence behavior of MBBE, MBCN and MBXAN, the geometric configuration of three luminogens were optimized at the B3LYP/def2-TZVP level, whose the highest occupied molecular orbitals (HOMO) and the lowest unoccupied molecular orbitals (LUMO) distributions, main energy levels and spin orbit coupling constants ( $\xi$ ) were calculated (Fig. 5). The electron cloud density of HOMO and LUMO orbitals of three luminogens was mainly distributed on the

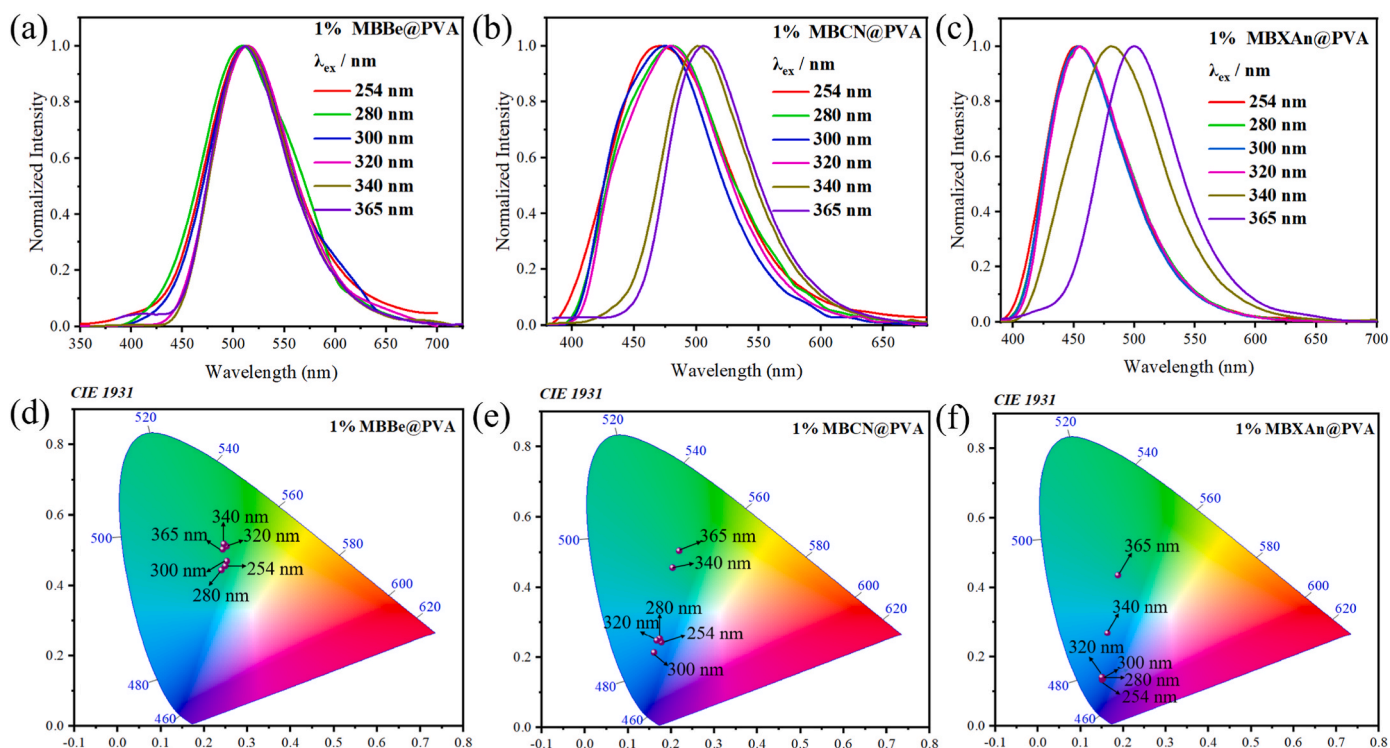


**Fig. 3.** (a)–(c) The normalized phosphorescence spectra of 1 % MBBe@PVA, 1 % MBCN@PVA and 1 % MBXAn@PVA films at different excitation wavelengths. (d)–(f) CIE chromaticity coordinates of 1 % MBBe@PVA, 1 % MBCN@PVA and 1 % MBXAn@PVA films at different excitation wavelengths.

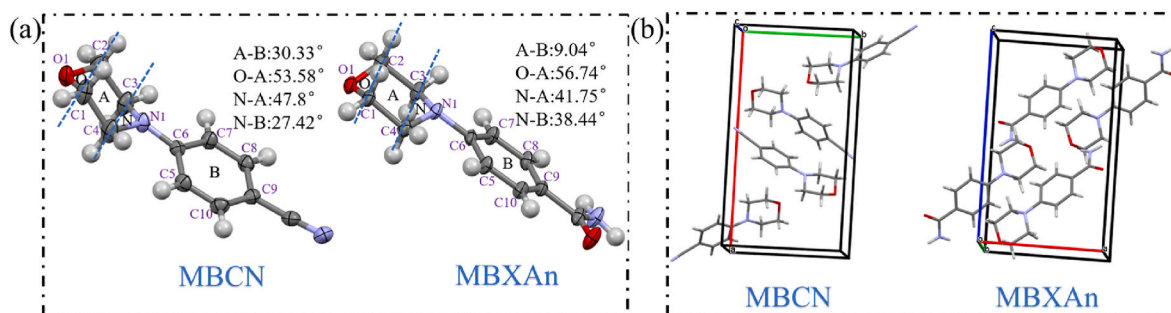


**Fig. 4.** (a) Molecular conformation and (b) the cell unit of crystals MBCN and MBXAn.

aromatic rings and N of morpholine unit, but obvious electron density migration could be observed from N of morpholine unit to the aromatic rings, indicating typical D-A type luminogens and intramolecular charge transfer (ICT) characteristics. Furthermore, the energy gaps between HOMO and LUMO were 4.336 eV, 4.699 eV, and 4.870 eV for MBBe, MBCN and MBXAn in turn, corresponding to the red shifted absorption maxima for MBBe than MBCN and MBXAn very well (Fig. 1a–c). The energy gap ( $\Delta E_{S_1T_2}$ ) of MBBe between  $S_1$  and  $T_2$  was 0.19 eV, with  $\xi(S_1 \rightarrow T_2)$  of  $0.354 \text{ cm}^{-1}$ , effectively promoting ISC and generation of triplet excitons. Moreover,  $\xi(T_1 \rightarrow S_0)$  related to phosphorescence radiation was  $0.531 \text{ cm}^{-1}$ . Similar to MBBe, MBCN also showed a main ISC channel from  $S_1 \rightarrow T_2$ , but with smaller  $\xi(S_1 \rightarrow T_2)$  ( $0.304 \text{ cm}^{-1}$ ) and  $\xi(T_1 \rightarrow S_0)$  ( $0.363 \text{ cm}^{-1}$ ), as well as a significantly reduced  $\Delta E_{S_1T_2}$  (0.06 eV). By contrast,  $\xi(S_1 \rightarrow T_2)$  of MBBe and MBCN was equivalent, but the significantly reduced  $\Delta E_{S_1T_2}$  and smaller  $\xi(T_1 \rightarrow S_0)$  were respectively beneficial for promoting the rapid formation of triplet excitons and the slower phosphorescence radiation for MBCN than MBBe. As a result, 1 % MBBe@PVA film exhibited higher RTP quantum yield ( $\Phi_p$ ) and shorter RTP and afterglow lifetimes than 1 % MBCN@PVA film (Table 2 and Fig. 2). Different from MBBe and MBCN, the main ISC channel of MBXAn

was  $S_1 \rightarrow T_1$  rather than  $S_1 \rightarrow T_2$ , which could avoid the relaxation process of MBBe and MBCN from  $T_2$  to  $T_1$  and thereby reduce non-radiative energy loss. Meanwhile, Dihedral angles of plane N–B were  $89.61^\circ$  and  $35.65^\circ$  in  $S_1$  and  $T_1$  states in sequence, which contributed to endowing  $S_1$  and  $T_1$  states more  $n-\pi^*$  and  $\pi-\pi^*$  transition characteristics respectively based on the twisted  $S_1$  state and relatively flattened  $T_1$  state (Fig. S27), yielding big  $\xi(S_1 \rightarrow T_1)$ . MBXAn had bigger  $\xi(S_1 \rightarrow T_1)$  ( $1.059 \text{ cm}^{-1}$ ) and  $\xi(T_1 \rightarrow S_0)$  ( $2.927 \text{ cm}^{-1}$ ) than MBBe and MBCN, and with a tiny  $\Delta E_{S_1T_1}$  (0.19 eV), which boosted the rapid formation and phosphorescence radiation of triplet excitons, corresponding to a significantly improved  $\Phi_p$  for 1 % MBXAn@PVA film than 1 % MBCN@PVA and 1 % MBBe@PVA films (Table 2). Subsequently, natural transition orbitals (NTOs) analysis was performed for MBBe, MBCN, and MBXAn at the  $S_1$ ,  $T_1$ , and  $T_2$  states (Fig. S31). The results revealed that the introduction of different substituents had an obvious impact on the nature of the electronic transitions. The three luminogens exhibited  $S_1$  states with predominantly  $^1(n, \pi)$  character. In contrast, MBBe showed  $T_1$  and  $T_2$  states with predominantly  $^3(\pi, \pi)$  and  $^3(n, \pi)$  characters, respectively, but  $T_1$  and  $T_2$  states of MBCN and MBXAn were characterized by predominant  $^3(\pi, \pi)$  characters. These differences led to

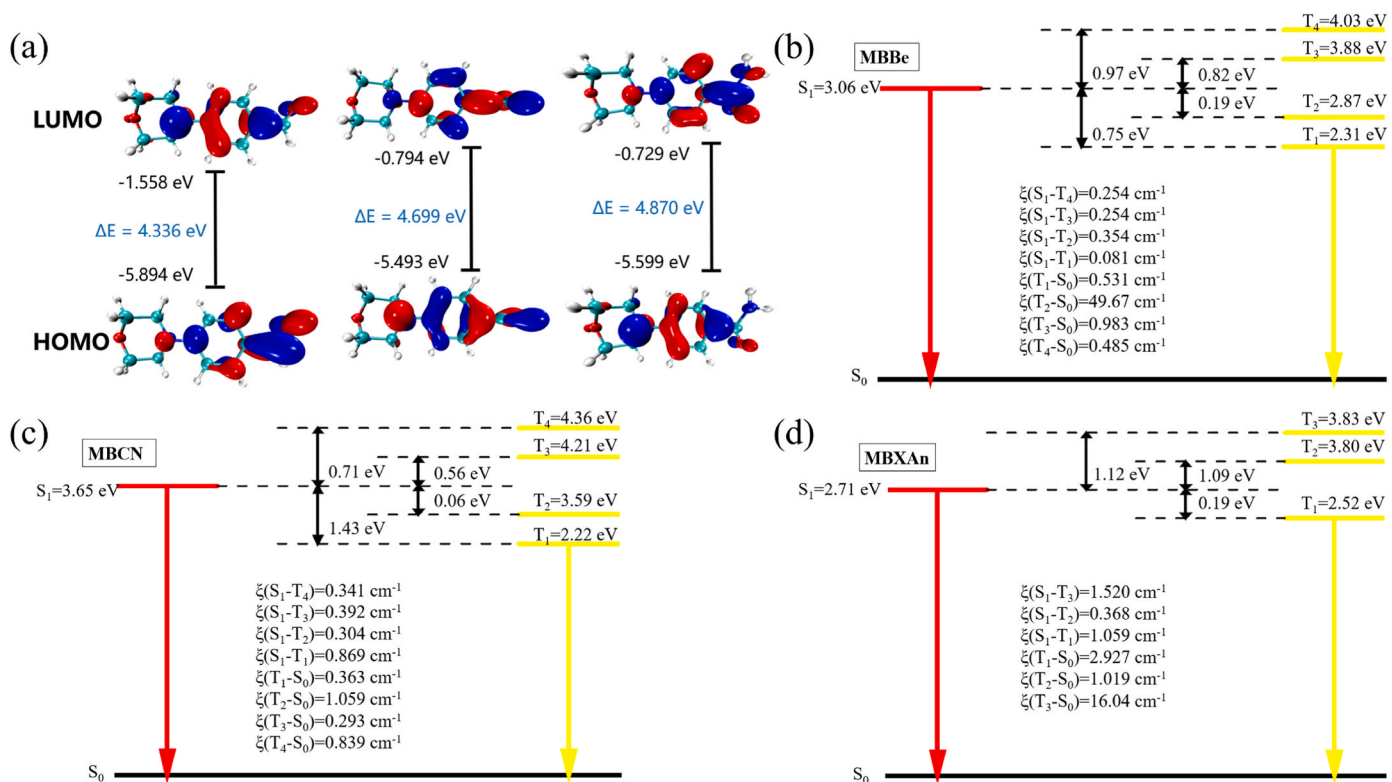


Fig. 5. (a) HOMO and LUMO distributions of MBBE, MBCN and MBXAn. (b) Energy levels and spin orbit coupling constants ( $\xi$ ) of MBBE, (c) MBCN and (d) MBXAn.

larger  $\xi(S_1 \rightarrow T_1)$  for MBCN and MBXAn compared to MBBE (Fig. 5). Of note, the above-mentioned data illustrates that three luminogens possess phosphorescence nature, while invisible afterglow for crystals MBBE and

MBCN should be attributed to molecular motions and oxygen quenching. Overall, the fine-tuning of electron acceptors not only affected intermolecular interactions, but also changed molecular conformations

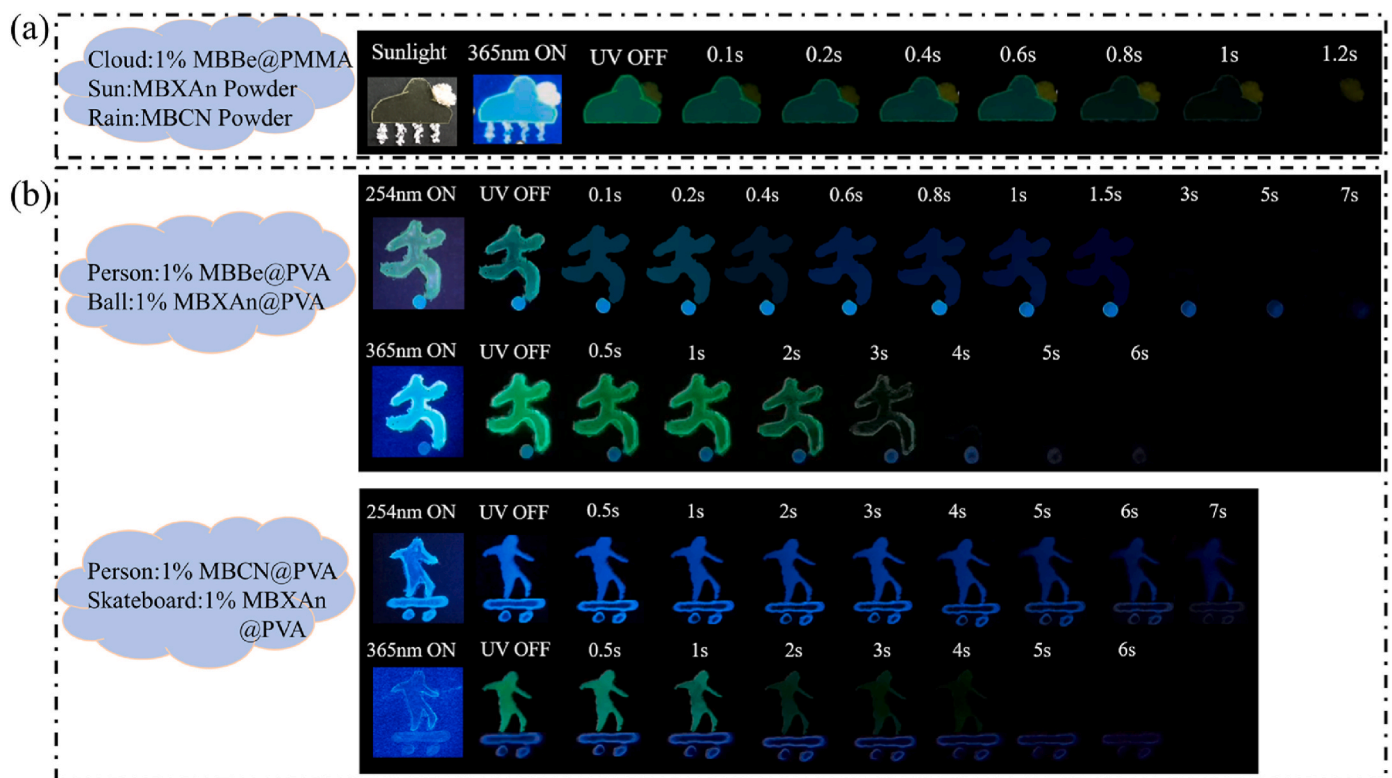


Fig. 6. Anti-counterfeiting application by using (a) 1% MBBE@PMMA film, MBCN and MBXAn Powder, (b) the 1% MBBE @PVA, 1% MBCN @PVA and 1% MBXAn @PVA doping systems.

of the ground state and excited states. Furthermore, the different twisted degrees between D and A units could tune  $n-\pi^*$  and  $\pi-\pi^*$  transition characteristics of excited states, leading to different ISC, phosphorescence radiative rate ( $K_p$ ) and  $K_{phnr}$ . Among of three luminogens, crystal MBXAn showed the best RTP performance ( $\Phi_p = 0.377$ ,  $\tau = 404.84$  ms) due to the enhanced intermolecular interactions, ISC, and phosphorescence radiation rates.

#### 4. Applications

Encryption is the process of converting plaintext information into ciphertext information, making it unreadable in the absence of special information and measures, which can effectively protect personal privacy, company and business secrets, and national security. Based on excitation dependent RTP and different RTP lifetimes of the dyes, a series of advanced encryption patterns were prepared. As shown in Fig. 6a, raindrops, cloud and sun were drawn respectively by MBCN Powder, 1 % MBBe@PMMA film (Fig. S28) and MBXAn Powder. Switching on-off 365 nm UV lamp, raindrops disappeared firstly, followed by cloud and sun, representing a weather transition process from rainy via cloudy to sunny day. Fig. 6b expressed the dynamic process of kicking and skateboarding from near to far. The person and ball were constructed by 1 % MBBe@PVA and 1 % MBXAn@PVA films in turn, in another picture, the person and skateboard were drawn by 1 % MBCN@PVA and 1 % MBXAn@PVA films respectively. By the switching on-off of 254 nm UV lamp, the person kicked the ball out in 1 s in a picture, which became 3 s after ceasing 365 nm UV lamp radiation. In another picture, the blue clothed person became a green clothed person on a blue skateboard by different UV lamp radiation.

#### 5. Conclusions

Based on NMR and HR-MS characterization, single-crystal X-ray diffraction, and HPLC analysis, molecular structures and purity of three D-A type luminogens were confirmed. By tuning electron acceptors, high contrast crystalline, dynamic, and excitation dependent RTP was achieved. Power and crystal MBXAn could present green afterglow, lasting for 2 s and 3 s in turn, whose RTP lifetimes and  $\Phi_p$  were 164.77 ms, 0.239, 404.84 ms, and 0.377 in sequence, indicating crystal enhanced RTP, while MBBe and MBCN gave invisible RTP in power and crystalline state. Crystal analysis and theoretical calculations provided a detailed underlying mechanism analysis for the above high contrast RTP, which indicated that MBXAn had stronger intermolecular interactions, as well as bigger  $\xi(S_1 \rightarrow T_1)$  and  $\xi(T_1 \rightarrow S_0)$  compared with MBBe and MBCN, leading to bright afterglow and high  $\Phi_p$  for crystal MBXAn, as well as longer unimolecular afterglow and high  $\Phi_p$  for 1 % MBXAn@PVA film than 1 % MBBe@PVA and 1 % MBCN@PVA films. 1 % MBBe@PVA and 1 % MBCN@PVA film presented excitation wavelength dependent blue or green afterglows due to different RTP emission and lifetimes between unimolecular and aggregated luminogens, while the pristine 1 % MBXAn@PVA film maintained blue afterglow under different excitation wavelengths because of the absence of aggregated RTP. Migration and aggregation of MBXAn in PVA film led to green afterglow of aggregated MBXAn and shortened afterglow lifetime. This work not only obtained a long-lived and efficient crystal RTP luminogen, screened an excellent electron acceptor for RTP chromophore, simultaneously possessing the enhanced intermolecular interactions and ISC abilities, but also provided an excellent platform for building advanced encryption patterns by high contrast crystalline, dynamic, and excitation dependent RTP.

#### CRediT authorship contribution statement

**Weirao Ji:** Writing – original draft, Supervision, Methodology, Investigation, Data curation. **Yupeng Zhao:** Writing – original draft, Software, Data curation. **Yang Zhu:** Writing – original draft,

Supervision, Methodology, Investigation, Data curation. **Lei Ma:** Writing – review & editing, Software, Methodology, Investigation. **Yongtao Wang:** Writing – review & editing, Resources, Project administration, Methodology, Investigation, Funding acquisition, Conceptualization.

#### Data availability

No data was used for the research described in the article.

#### Declaration of competing interest

The authors declare that they have no known competing financial interests or personal relationships that could have appeared to influence the work reported in this paper.

#### Acknowledgment

This work was supported by the Guangxi Natural Science Foundation (Grant No. 2024GXNSFAA999457 and 2020GXNSFAA159147), the National Natural Science Foundation of China (Grant No. 21766030).

#### Appendix A. Supplementary data

Supplementary data to this article can be found online at <https://doi.org/10.1016/j.dyepig.2025.112852>.

#### Data availability

The authors do not have permission to share data.

#### References

- Cardeynals T, Paredis S, Danos A, Harrison A, Deckers J, Brebels S, et al. Difluorodithieno[3,2-a:2',3'-c]phenazine as a strong acceptor for materials displaying thermally activated delayed fluorescence or room temperature phosphorescence. *Dyes Pigm* 2021;190:109301. <https://doi.org/10.1016/j.dyepig.2021.109301>.
- Jiang D, Du C, Yan Z, Ge S, Feng Z, Wan L, et al. Modulating room temperature phosphorescence through intermolecular halogen bonding. *J Mater Chem C* 2023; 11:4203–9. <https://doi.org/10.1039/d2tc05237g>.
- Ding B, Ma X, Tian H. Recent advances of pure organic room temperature phosphorescence based on functional polymers. *Acc Mater Res* 2023;4:827–38. <https://doi.org/10.1021/accountsmr.3c00090>.
- Song T, Liu H, Ren J, Wang Z. Achieving TADF and RTP with stimulus-responsiveness and tunability from phenothiazine-based donor–acceptor molecules. *Adv Opt Mater* 2023;12:2301215. <https://doi.org/10.1002/adom.202301215>.
- Guo J, Zhao Y, Ma L, Wang Y. Ultra-long room temperature phosphorescence, intrinsic mechanisms and application based on host-guest doping systems. *Chin J Struct Chem* 2024;43:100335. <https://doi.org/10.1016/j.cjcs.2024.100335>.
- Liu Y, Yang H, Huang H, Niu L, Liu S. Recent advances of biomass-derived carbon dots with room temperature phosphorescence characteristics. *Nano Today* 2024; 56:102257. <https://doi.org/10.1016/j.nantod.2024.102257>.
- Stanitska M, Volyniuk D, Minaev B, Agren H, Grazulevicius J V. Molecular design, synthesis, properties, and applications of organic triplet emitters exhibiting blue, green, red and white room-temperature phosphorescence. *J Mater Chem C* 2024; 12:2662–98. <https://doi.org/10.1039/d3tc04514e>.
- Tian Y, Yang J, Liu Z, Gao M, Li X, Che W, et al. Multistage stimulus-responsive room temperature phosphorescence based on host-guest doping systems. *Angew Chem Int Ed* 2021;60:20259–63. <https://doi.org/10.1002/anie.202107639>.
- Wang Y, Gao H, Yang J, Fang M, Ding D, Tang B, et al. High performance of simple organic phosphorescence host-guest materials and their application in time-resolved bioimaging. *Adv Mater* 2021;33:2007811. <https://doi.org/10.1002/adma.202007811>.
- Zhang Y, Sun Q, Yue L, Wang Y, Cui S, Zhang H, et al. Room temperature phosphorescent (RTP) thermoplastic elastomers with dual and variable RTP emission, photo-patterning memory effect, and dynamic deformation RTP response. *Adv Sci* 2022;9:2103402. <https://doi.org/10.1002/adv.202103402>.
- Zhao Y, Yang J, Liang C, Wang Z, Zhang Y, Li G, et al. Fused-ring pyrrole-based near-infrared emissive organic RTP material for persistent afterglow bioimaging. *Angew Chem Int Ed* 2024;63:e202317431. <https://doi.org/10.1002/anie.202317431>.
- Zhou W, Lin W, Chen Y, Liu Y. Supramolecular assembly confined purely organic room temperature phosphorescence and its biological imaging. *Chem Sci* 2022;13: 7976–89. <https://doi.org/10.1039/d2sc01770a>.

- [13] Jiang G, Li Q, Lv A, Liu L, Gong J, Ma H, et al. Modulation of the intramolecular hydrogen bonding and push-pull electron effects toward realizing highly efficient organic room temperature phosphorescence. *J Mater Chem C* 2022;10:13797–804. <https://doi.org/10.1039/d2tc01093c>.
- [14] Jiang J, Liu J, Hu C, Wang Y, Ma L. Construction and fine tuning of host-guest doping systems and the underlying mechanism of room temperature phosphorescence. *Dyes Pigm* 2024;222:111931. <https://doi.org/10.1016/j.dyepig.2023.111931>.
- [15] Ma L, Ma X. Recent advances in room-temperature phosphorescent materials by manipulating intermolecular interactions. *Sci China Chem* 2022;66:304–14. <https://doi.org/10.1007/s11426-022-1400-6>.
- [16] Ma X, Wang J, Tian H. Assembling-induced emission: an efficient approach for amorphous metal-free organic emitting materials with room-temperature phosphorescence. *Acc Chem Res* 2019;52:738–48. <https://doi.org/10.1021/acs.accounts.8b00620>.
- [17] Xiong Y, Zhao Z, Zhao W, Ma H, Peng Q, He Z, et al. Designing efficient and ultralong pure organic room-temperature phosphorescent materials by structural isomerism. *Angew Chem Int Ed* 2018;57:7997–8001. <https://doi.org/10.1002/anie.201800834>.
- [18] Shi L, Li X, Wang Y, Ma L. Single component long-lived dynamic room temperature phosphorescence with large-scale preparation and visible light excitation. *J Mol Struct* 2024;1311:138434. <https://doi.org/10.1016/j.molstruc.2024.138434>.
- [19] Xu X, Yan B. Recent advances in room temperature phosphorescence materials: design strategies, internal mechanisms and intelligent optical applications. *Phys Chem Chem Phys* 2023;25:1457–75. <https://doi.org/10.1039/d2cp05063c>.
- [20] Zhai Y, Li S, Li J, Liu S, James T, Sessler J, et al. Room temperature phosphorescence from natural wood activated by external chloride anion treatment. *Nat Commun* 2023;14:2614. <https://doi.org/10.1038/s41467-023-37762-9>.
- [21] Wang T, Gupta A, Wu S, Slawin A, Zysman-Colman E. Conjugation-modulated excitonic coupling brightens multiple triplet excited states. *J Am Chem Soc* 2023;145:1945–54. <https://doi.org/10.1021/jacs.2c12320>.
- [22] Dai W, Bianconi T, Ferraguzzi E, Wu X, Lei Y, Shi J, et al. Excited-state modulation of aggregation-induced emission molecules for high-efficiency triplet exciton generation. *ACS Mater Lett* 2021;3:1767–77. <https://doi.org/10.1021/acsmaterialslett.1c00528>.
- [23] Ding H, Sun Y, Tang M, Wen J, Yue S, Peng Y, et al. Time-dependent photo-activated aminoborane room-temperature phosphorescence materials with unprecedented properties: simple, versatile, multicolor-tunable, water resistance, optical information writing/erasing, and multilevel data encryption. *Chem Sci* 2023;14:4633–40. <https://doi.org/10.1039/d3sc00568b>.
- [24] Guo J, Liu J, Zhao Y, Wang Y, Ma L, Jiang J. Time-dependent and clustering-induced phosphorescence, mechanochromism, structural-function relationships, and advanced information encryption based on isomeric effects and host-guest doping. *Spectrochim Acta Mol Biomol Spectrosc* 2024;317:124449. <https://doi.org/10.1016/j.saa.2024.124449>.
- [25] Lv X, Cao X, Wu H, Lin H, Ni F, Huang H, et al. Realize efficient organic afterglow from simple halogenated acridan derivatives. *Chem Eng J* 2021;419:129598. <https://doi.org/10.1016/j.cej.2021.129598>.
- [26] Sun Y, Qu H, Zhang J, Duan X, Zhang X. Room temperature phosphorescence, thermally activated delayed fluorescence and multicolor mechanochromic luminescence of emitters through molecular interaction and conformational modulations. *Tetrahedron* 2022;110:132692. <https://doi.org/10.1016/j.tet.2022.132692>.
- [27] Zhang K, Dan N, Ren D, Zhang R, Lu X, Wu Y, et al. A small D-A molecule with highly heat-resisting room temperature phosphorescence for white emission and anti-counterfeiting. *Chin J Struct Chem* 2024;43:100244. <https://doi.org/10.1016/j.cjsc.2024.100244>.
- [28] Zhong D, Liu S, Yue L, Feng Z, Wang H, Yang P, et al. Achieving pure room temperature phosphorescence (RTP) in phenoselenazine-based organic emitters through synergism among heavy atom effect, enhanced  $n \rightarrow \pi^*$  transitions and magnified electron coupling by the A–D–A molecular configuration. *Chem Sci* 2024;15:9112–9. <https://doi.org/10.1039/d4sc01200c>.
- [29] Gao Q, Shi M, Chen M, Hao X, Chen G, Bian J, et al. Facile preparation of full-color tunable room temperature phosphorescence cellulose via click chemistry. *Small* 2024;20:2309131. <https://doi.org/10.1002/sml.202309131>.
- [30] Xiang J, Shi Y, Jiang J, Yan J, Xiao S, Lin H, et al. Color-tunable room temperature afterglow of non-conventional organogels for dynamic anti-counterfeiting. *Adv Opt Mater* 2023;12:2302671. <https://doi.org/10.1002/adom.202302671>.
- [31] Peng F, Chen Y, Liu H, Chen P, Peng F, Qi H. Color-tunable, excitation-dependent, and water stimulus-responsive room-temperature phosphorescence cellulose for versatile applications. *Adv Mater* 2023;35:2304032. <https://doi.org/10.1002/adma.202304032>.
- [32] Zhang Z, Wang Z, Liu X, Shi Y, Li Z, Zhao Y. Modulating emission of boric acid into highly efficient and color-tunable afterglow via dehydration-induced through-space conjugation. *Adv Sci* 2023;10:2300139. <https://doi.org/10.1002/advs.202300139>.
- [33] Dou X, Zhu T, Wang Z, Sun W, Lai Y, Sui K, et al. Color-tunable, excitation-dependent, and time-dependent afterglows from pure organic amorphous polymers. *Adv Mater* 2020;32:2004768. <https://doi.org/10.1002/adma.202004768>.
- [34] Gao Q, Shi M, Rao J, Su Z, Chen G, Lü B, et al. Fully exploiting clusterization-triggered room temperature phosphorescence of cellulose by stepwise rigidification for long-lived and excitation wavelength-dependent afterglows. *Adv Funct Mater* 2024;34:2403977. <https://doi.org/10.1002/adfm.202403977>.
- [35] Wang F, Zhou S, Zhang Y, Wang Y, Guo R, Xiao H, et al. Chiral phosphorescent carbonized polymer dots relayed light-harvesting system for color-tunable circularly polarized room temperature phosphorescence. *Small* 2024;20:2306969. <https://doi.org/10.1002/sml.202306969>.
- [36] Cai X, Gao B, Li X, Cao Y, Su S. Singlet-triplet splitting energy management via acceptor substitution: explanation molecular design for deep-blue thermally activated delayed fluorescence emitters and organic light-emitting diodes application. *Adv Funct Mater* 2016;26:8042–52. <https://doi.org/10.1002/adfm.201603520>.
- [37] Shi L, Liu J, Ma L, Wang Y. The dual-band emission with long-lived thermally activated delayed fluorescence and room temperature phosphorescence by trace ingredient incorporation. *Chem Eng J* 2024;493:152492. <https://doi.org/10.1016/j.cej.2024.152492>.
- [38] Gao Y, Zhang H, Shuang S, Dong C. Visible-light-excited ultralong-lifetime room temperature phosphorescence based on nitrogen-doped carbon dots for double anticounterfeiting. *Adv Opt Mater* 2020;8:1901557. <https://doi.org/10.1002/adom.201901557>.
- [39] Xie W, Huang W, Li J, He Z, Huang G, Li B, et al. Anti-kasha triplet energy transfer and excitation wavelength dependent persistent luminescence from host-guest doping systems. *Nat Commun* 2023;14:8098. <https://doi.org/10.1038/s41467-023-43687-0>.
- [40] Zhou Q, Yang C, Zhao Y. Dynamic organic room-temperature phosphorescent systems. *Chem* 2023;9:2446–80. <https://doi.org/10.1016/j.chempr.2023.05.023>.
- [41] Jiang D, Lu T, Du C, Liu F, Yan Z, Hu D, et al. Utilizing morpholine for purely organic room temperature phosphors. *Sci China Chem* 2023;66:1132–8. <https://doi.org/10.1007/s11426-022-1507-2>.
- [42] Zhang C, Lou L, Li Y, Sun S, Hu W, Wang K, et al. Highly efficient organic host/guest phosphorescent system with tunable lifetime and color. *J Phys Chem C* 2023;127:20929–38. <https://doi.org/10.1021/acs.jpcc.3c05354>.
- [43] Zhu Y, Pan M, Ma L, Wang Y. The luminescence mechanism of two pure organic room temperature phosphorescent isomers, mechanical force detection, 3D modeling, and dynamic data encryption. *Chem Eng J* 2025;505:159245. <https://doi.org/10.1016/j.cej.2025.159245>.
- [44] Wang H, Jin L, Mo W, Hong W. Dynamic encryption enabled by circularly polarized carbon dot-based afterglow composites featuring hierarchical tri-mode thermochromic emission. *Chem Eng J* 2025;512:162427. <https://doi.org/10.1016/j.cej.2025.162427>.
- [45] Feng H, Gao W, Li D, Su Z. Stimulus-responsive organic room temperature phosphorescence materials based on host-guest doping systems. *J Mol Struct* 2025;1334:141897. <https://doi.org/10.1016/j.molstruc.2025.141897>.
- [46] Zhao X, Shuai S, Wang R, Peng F, Kong X, Shi W. Excitation wavelength-dependent room temperature phosphorescence based on dual confinement of an organic-inorganic matrix for dynamic information encryption. *Dalton Trans* 2025;54:5880–7. <https://doi.org/10.1039/d5dt00123d>.
- [47] Zhang BL, Miao L, Song WT, Zhang JJ, Chen J, Wang T, et al. Precisely regulating photoactivated dynamic room temperature phosphorescence by alkyl chain-induced lattice-softening. *Adv Funct Mater* 2025;35:2415094. <https://doi.org/10.1002/adfm.202415094>.